

Using self-driven microswimmers for particle separation

W. Yang^{1,2}, V. R. Misko¹, K. Nelissen^{1,3}, M. Kong⁴, and F. M. Peeters^{1,3}

¹*Departement Fysica, Universiteit Antwerpen, Groenenborgerlaan 171, B-2020 Antwerpen, Belgium*

²*College of Materials Science and Engineering, Taiyuan University of Science and Technology, Taiyuan 030024, P. R. China*

³*Departamento de Física, Universidade Federal do Ceará,*

Caixa Postal 6030, Campus do Pici, 60455-760 Fortaleza, Ceará, Brazil

⁴*Institute of Plasma Physics, Chinese Academy of Sciences, Hefei 230031, P. R. China*

(Dated: October 10, 2018)

Microscopic self-propelled swimmers capable of autonomous navigation through complex environments provide appealing opportunities for localization, pick-up and delivery of micro- and nanoscopic objects. Inspired by motile cells and bacteria, man-made microswimmers have been fabricated, and their motion in patterned surroundings has been experimentally studied. We propose to use self-driven artificial microswimmers for separation of binary mixtures of colloids. We revealed different regimes of separation including one with a velocity inversion. Our finding could be of use for various biological and medical applications.

PACS numbers: 36.40.Wa, 82.70.Dd, 87.15.hj

I. INTRODUCTION

Quasi-one-dimensional (Q1D) colloidal systems play an increasingly important role as model systems to study a variety of collective phenomena in low dimensional condensed matter physics. The well-controlled way in real space and time, and the tunable interparticle interaction potential of colloidal systems lead to insights of a wide range of systems. Most of the studies on Q1D colloidal systems focused on stripe structures and crystal defects [1–4], solid-liquid phase transitions [5, 6], single-file diffusion [7–10] and transport behavior under external driving force [11–14], including, e.g., dragged particles [15]. Transport properties of colloidal particles driven by an external force in narrow channels became a growing topic during the last decade. This is by part because the transport behavior might provide a deeper understanding of several biological systems, e.g., ion-channel transport in cell membranes [16, 17], DNA manipulations and separations [18–20]. Also it is a readily available physical model to mimic other types of particles, including different ions and electrons, which might lead to practical use in microdevices and nanodevices [21, 22]. Moreover, the transport behaviors are important in real systems of medicine, food production and field-response materials as well. There are also studies of transport properties of particles which are driven in other shapes of patterned environments [23, 24].

In nature and technology, many systems are mixtures of different particle types. The distinction and interaction, mixture and separation of each particle type give rise to an exceedingly rich phenomenology as compared to monodisperse systems. This motivated a number of studies on complex mixtures and, in particular, binary mixtures (see, e.g., [25–30]).

One of the fundamental problems related to binary mixtures is their separation (see, e.g., [25–29]). This problem is commonly tackled by using different asymmetric potentials for separating, e.g., interacting binary

mixtures driven on periodic substrates [25–29]) or ferrofluids [31]. Mixtures of particles can be driven either along the symmetry axis of the potentials, or in the transverse direction [32] which was demonstrated in the context of separation of macromolecules, DNA, or even cells (see, e.g., [33–37]).

Note that in the previous studies a driving force (e.g., gravity [12] or external field [11, 13, 14]) was applied to *all* the particles of the system (or to one of the species), and the separation occurred either due to the different dynamic response of the species to the driving/potentials or due to their different self-diffusion constant.

In contrast to that, here we propose a new mechanism of particle separation. It is based on injecting special particles which are able to move in the binary mixture and interact with its species. These can be either particles driven by external forces (which describes a typical situation in microrheology [38]) or *self-driven* particles i.e., driven by various self-phoretic forces produced by a chemical (self-chemophoresis) (see, e.g., the recent review paper [39]), electrical (self-electrophoresis) or thermal (self-thermophoresis) gradient that the particle generates around itself (see Ref. [40] and references therein). For example, so-called Janus particles (μm -sized particles covered by gold on one of the hemispheres) can move (“swim”) when being illuminated by light (details of the mechanism of motion of these artificial “microswimmers” (MS) are beyond the scope of this work and can be found in [40, 41]). Due to their amphiphilicity, Janus particles are extensively studied as a model of structure-directing amphiphiles (see, e.g., [42]) and in relation to their applications in new functional materials (see, e.g., [43, 44]). Here we demonstrate that artificial MS, when moving in a binary mixture, are capable of *selectively driving* and separating the flows of different species of the binary mixture.

II. SIMULATION

We consider a binary system of paramagnetic colloidal particles confined in a 2D infinitely long narrow hard-wall channel in an external perpendicular magnetic field. The particles (including the microswimmer — for experimental realization of paramagnetic microswimmers see Refs. [45, 46]) interact via a repulsive dipole-dipole potential (see, e.g., experiments [3, 12]) $V_{ij}(\vec{r}_i, \vec{r}_j) = Q_i Q_j / |\vec{r}_i - \vec{r}_j|^3$, where $Q_i = M_i \sqrt{\mu_0 / 4\pi}$ is the “effective charge”, M_i is the magnetic moment, and \vec{r}_i is the coordinate of the i -th particle; μ_0 is the magnetic permeativity. We assume that there are two types of particles, A and B, which differ by size and charge. We call them “small” (A) and “big” (B) particles. The system consists of N_A small particles with Q_A , and N_B big particles with $Q_B = 8Q_A$. The effective charge of self-driven MS is chosen $Q_d = Q_A$. We introduce a unit energy $E_0 = Q_A^2 / a_0^3$ of the inter-particle interaction $V_{ij}(\vec{r}_i, \vec{r}_j)$, where the unit length $a_0 = 10 \mu\text{m}$ is on the order of the average distance between particles [3, 12]. Thus the inter-particle interaction can be characterized by the dimensionless coupling parameter $\Gamma = Q_A^2 / a_0^3 k_B T$, where k_B is the Boltzmann constant and T the ambient temperature. In our simulations, we choose $\Gamma = 200$ which corresponds to the strongly correlated regime, i.e., below the melting transition. Correspondingly, the unit force is $F_0 = \Gamma k_B T / a_0$. For the chosen $\Gamma = 200$ and room temperature, $F_0 = 8.28 \cdot 10^{-14}$ N.

The motion of colloidal particles is investigated using the Langevin equations of motion in the overdamped regime, i.e., the Brownian dynamics (BD) method. This approach neglects hydrodynamic interactions as well as the short-time momentum relaxation of the particles (see, e.g., [12, 13, 47]). The overdamped equations of motion of particles are:

$$\frac{d\vec{r}_i}{dt} = \frac{D_i}{k_B T} \left\{ -\nabla_{\vec{r}_i} \sum_{i \neq j} V_{ij}(\vec{r}_i, \vec{r}_j) + \vec{F}_{drx} + \tilde{F}_i(t) \right\}, \quad (1)$$

where D_i is the self-diffusion coefficient, which is chosen as $D_i^A = 1.0 \mu\text{m}^2/\text{s}$ for type A (and for MS) and $D_i^B = 0.7 \mu\text{m}^2/\text{s}$ for type B particles, according to the experiment [12, 41]. The first term of the rhs of Eq. (1) is the sum of all repulsive interaction forces acting on each particle, the second term is the “self-driving force” acting *only* on the MS (or “motor” particle [48, 49]). Recently, a similar approach has been used for the description of motion of swimming bacteria and self-driven particles [50]. Note that force \vec{F}_{drx} entering into the Langevin equation (1) is an effective force which describes the propulsion mechanism on average (see, e.g., the recent studies [51, 52] on the Brownian motion of a self-propelled particle). In experiment, this effective “driving force” can be tuned by, e.g., changing the intensity of the incident light (in case of Janus particles), the geometry of the experiment [41], or the number of MS particles, etc.; we do not discuss here the relation between \vec{F}_{drx} and those

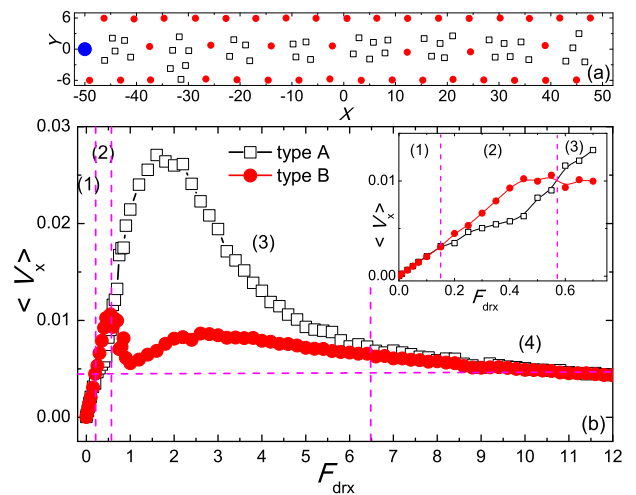


FIG. 1: (a) Equilibrium configuration of a system with equal number of particles of the two species $N_A = 40$, $N_B = 40$ and $Q_d = 8Q_A$. (b) The average velocity of particles of type A, $\langle V_x^A \rangle$ (black open squares connected by solid lines) and B, $\langle V_x^B \rangle$ (red dots connected by lines), as a function of F_{drx} . The microswimmer (MS) is shown by a blue filled circle. The same symbols are used in Figs. 2 to 5. The inset shows a zoom of the inversion velocity region (2).

parameters. Furthermore, without loss of generality we consider here only the x -component of \vec{F}_{dr} . This is justified by the fact that the (average) *direction* of motion of a MS (i.e., a Janus particle illuminated by light) can be controlled by, e.g., direction of the incident light and by using different illumination patterns [40, 41], or by additionally applied drift force [41]. Furthermore, in our case the motion of a MS across the channel is restricted by the boundaries. For simplicity, we ignore rotational motion of a MS [53]. The last term is the thermal random force that obeys the following conditions: $\langle \tilde{F}_i(t) \rangle = 0$, and $\langle \tilde{F}_{i\alpha}(t) \tilde{F}_{j\beta}(t') \rangle = 2 (k_B^2 T^2 / D_i) \delta(t - t') \delta_{ij} \delta_{\alpha\beta}$.

As a simulation cell, we use a unit box of length $L_x = 100$ (1mm) and width $L_y = 12$ (120 μm) (the box dimensions are close to those in the experiments [3, 12]). Periodic boundary conditions (PBC) are imposed in the x direction, and hard wall boundaries in the y direction. We use a cutoff ($r = 6$) for the dipole short-range inter-particle interaction. We also checked that by doubling the length of the simulation cell our results do not change.

The initial equilibrium configurations of the system were calculated for $\vec{F}_{drx} = 0$. Typical equilibrium distribution is shown in Fig. 1(a) for $N_A = N_B = 40$ and $N_{MS} = 1$, which is consistent with our previous results [30] (without MS particle; note that in our present simulations $N_{MS} \ll N_A, N_B$). Then we calculated the average velocities of A and B particles as a function of \vec{F}_{drx} . Simulations were typically performed for 10^8 time steps $\Delta t = 10^{-4}$ (s).

III. SEPARATION OF THE PARTICLE FLOWS

The average velocity (along the channel) $\langle V_x \rangle$ of particles A and B versus F_{drx} is shown in Fig. 1(b) for a typical system with $N_A = N_B = 40$. The main characteristic feature of the function $\langle V_x \rangle(F_{drx})$ is a well-pronounced particle flow separation for a broad range of F_{drx} . Note that particles A (small) move *faster* than their counterpart. Depending on F_{drx} , we can distinguish four different regions (shown in Fig. 1(b) as (1) to (4)).

Region (1): Rigid body motion

This regime corresponds to very small F_{drx} when the system is in a “rigid body” motion, i.e., velocities $\langle V_x^A \rangle$ and $\langle V_x^B \rangle$ coincide. The system is in a solid state ($\Gamma = 200$), and only elastic deformations are present [13].

Region (2): Inverse velocity motion

This regime is observed for small F_{drx} when the velocity of the MS is high enough to locally melt the solid, however, the velocities are inverted as compared to the broad region (3), i.e., particles A (small) move *slower* than particles B. This unusual behavior is explained by the stronger interaction of the MS with particles B than with particles A. As a consequence, particles B are carried along by the MS while the dynamical friction due to the particle motion is very small in this case and can be neglected. This regime is further illustrated in Fig. 2. The snapshots (Figs. 2(a-c)) show that the system adjusts itself to the slow “swimming” of the MS, without appreciable changes in the structure. However, the local density profile (Fig. 2(d)) indicates that the local density of particles B in front of the moving MS is higher than that of particles A. This means that particles B (big) are carried along by the MS while particles A (which interact weaker with the MS) “slip” and thus move slower.

Region (3): Strong flow separation

This regime is observed for a broad range of intermediate F_{drx} : this is the main and the most robust regime. With increasing velocity, the dynamical friction becomes increasingly important, and, as a result, type A particles (which are characterized by a larger self-diffusion coefficient) start to move faster. The function $\langle V_x^A \rangle(F_{drx})$ reaches its maximum at about $F_{drx} = 2$ and then gradually decreases while the function $\langle V_x^B \rangle(F_{drx})$ increases only slowly in this region and then decreases. It is worth noting that in this regime, the function $\langle V_x^B \rangle(F_{drx})$ first rapidly decreases. This decrease is accompanied by a simultaneous sharp increase in the function $\langle V_x^A \rangle(F_{drx})$. The origin of this behavior is explained by the fact that the motion of the two species (i.e., particles A and B) becomes less correlated as compared to that in regime (2). This loss of correlation in motion of the different species resembles the transition from elastic to plastic motion. The observed splitting of the average velocities is similar to the splitting in the velocities of adjacent layers found in a “vortex Wigner solid” [54, 55] where the transition to plastic motion was induced by shear stress. The snapshots and the local density profiles shown in Fig. 3 illus-

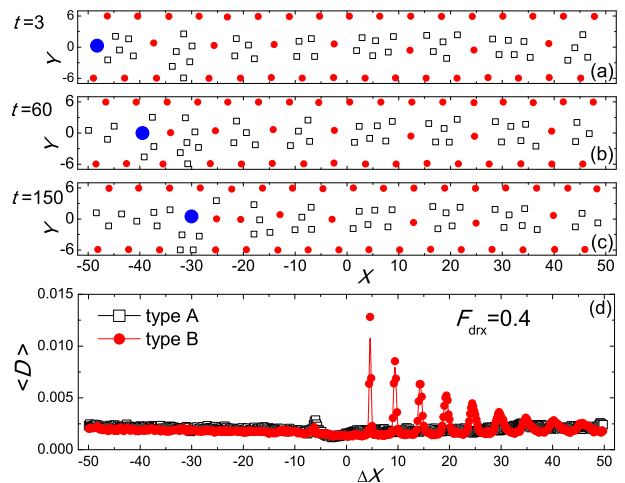


FIG. 2: (a-c) Snapshots of the configurations of the binary system (small particles of type A are shown by empty black squares; large particles of type B are shown by red dots) in presence of a microswimmer (shown by a blue filled circle), for $N_A = 40$, $N_B = 40$, $Q_d = 8Q_A$ and $F_{drx} = 0.4$, which corresponds to Regime (2) (see Fig. 1) of inverse velocities. The snapshots are recorded at $t = 3$ (a), 60 (b), and 150 (c). (d) The local density distribution of the particles versus distance to the MS, ΔX .

trate this regime. In contrast to regime (2) (cp. Fig. 2), the motion of the MS strongly influences the particle distribution: in particular, we observe a pronounced effect of particle separation in real space (i.e., not only in velocity space), or the formation of *clusters* of particles A which “trap” the MS and follow it (see Figs. 3(b, c)). The local density of particles A has a sharp peak in front of the MS (Fig. 3(d)), due to the MS-induced compression of the particle configuration in front of the MS. At the same time, the particles behind the MS are relaxed resulting in no peak in the local density.

Region (4): Fast MS motion.

This regime corresponds to large F_{drx} : finally, the system undergoes a transition to a “quasi-rigid body” regime when the MS moves too fast through the binary solid to produce a response in form of flow separation.

In order to analyze the role of the width of the channel, we performed simulations for wider channels, and we found that the effect of separation remains qualitatively similar: for a broad range of F_{dr} , the average velocity of small particles, $\langle V_x^A \rangle(F_{drx})$, is larger than that of large particles, $\langle V_x^B \rangle(F_{drx})$. However, the more gentle effect of velocity inversion can disappear, depending on the concentration of the particles. The role of imbalance in properties of the particles is discussed in the next section.

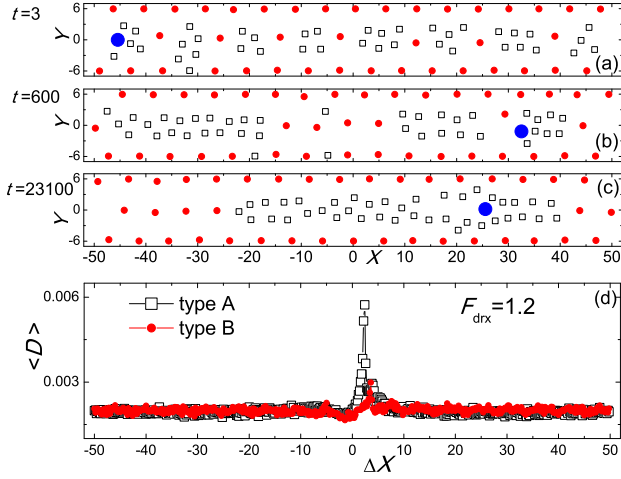


FIG. 3: (a-c) Snapshots of the configurations of the binary system in presence of a microswimmer (the same symbols are used as in Fig. 2), for $N_A = 40$, $N_B = 40$, $Q_d = 8Q_A$ and $F_{drx} = 1.2$, which corresponds to Regime (3) (see Fig. 1) of strong flow separation. The snapshots are recorded at $t = 3$ (a), 600 (b), and 23100 (c). (d) The local density distribution of the particles versus distance to the MS, ΔX .

IV. ROLE OF IMBALANCE IN PARTICLE PROPERTIES

Above, we revealed the general features of the separation of the particle flows by the MS “swimming” in a binary mixture and explained the mechanisms of the observed effect for the different separation regimes. Here we analyze the influence of the imbalance in particle properties, i.e., differences in charge of the MS and the constituent particles and the relative density of particles, on the observed effect.

We systematically examined systems with the charge of the MS varying in a broad range from $Q_d = Q_A$ to $Q_d = 128Q_A$. The results of our calculation of $\langle V_x \rangle$ versus F_{drx} for $Q_d = 2Q_A$, $12Q_A$, and $128Q_A$ are presented in Figs. 4(a-c). These results show that the position of the maximum average velocity $\langle V_x^A \rangle$ shifts towards larger F_{drx} with increasing the Q_d/Q_A ratio. We explain this by the fact that increasing the interparticle interaction enables the system response to the motion of the MS even for large velocities, with simultaneous extension of the initial rigid-body region (see Fig. 4(c)). Note that the region of inverted velocities exists only for a certain range of values of $Q_d/Q_A \sim 10$.

We analyzed the maximum effect of flow separation, i.e., the ratio $\langle V_x^A \rangle / \langle V_x^B \rangle \equiv VR_{max}$ and calculated its dependence on Q_d/Q_A (Fig. 4(d)): the initial fast grow is followed by a wide “plateau” (for $Q_d/Q_A = 10$ to 60) where $\langle V_x^A \rangle / \langle V_x^B \rangle \approx 4$, then followed by a considerable increase for $Q_d/Q_A > 60$.

We also studied the role of the imbalance in the density of particles A and B on the flow separation. We

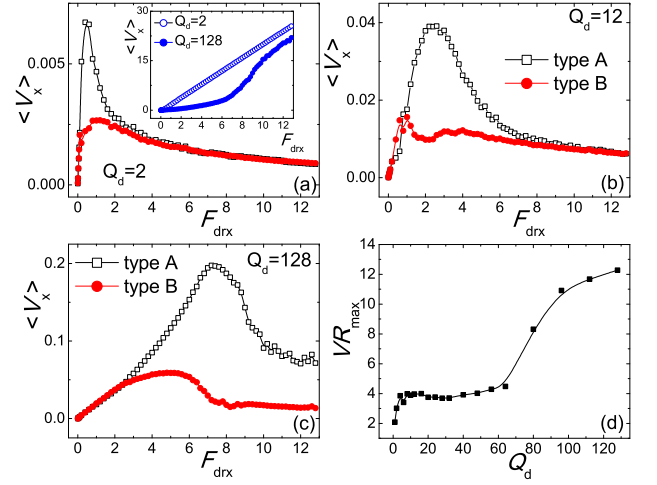


FIG. 4: (a-c) The average velocity ($\langle V_x \rangle$) of particles A and B as function of F_{drx} for a system with $N_A = N_B = 40$ and different charge of the MS, $Q_d = 2Q_A$ (a), $12Q_A$ (b), and $128Q_A$ (c). The inset in (a) shows the velocity of the driven apticle versus F_{drx} for systems with $Q_d = 2Q_A$ and $Q_d = 128Q_A$. (d) The maximum ratio of the velocities of particles A and B, VR_{max} , as a function of charge of the MS, Q_d .

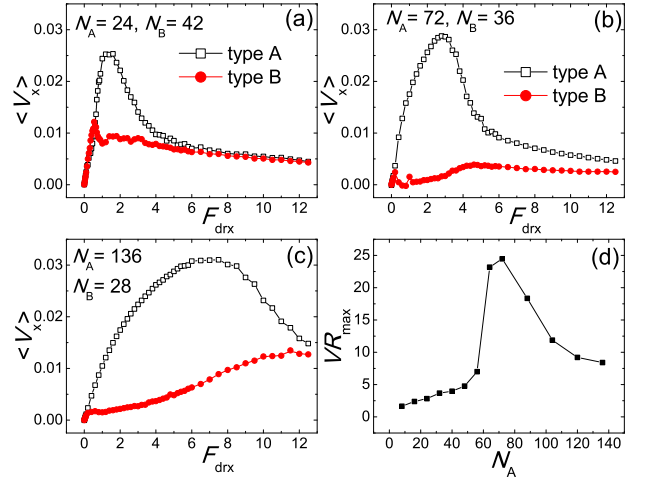


FIG. 5: (a-c) The function $\langle V_x \rangle$ for particles A and B versus the driving force for a system with $Q_d = 8Q_A$ and different relative densities of particles A and B. (d) The maximum ratio of the velocities of particles A and B, VR_{max} , as a function of number of particles A, N_A .

found that the position of the maximum of $\langle V_x^A \rangle$ shifts towards larger F_{drx} with increasing the N_A/N_B ratio. At the same time, the maximum effect of flow separation, $\langle V_x^A \rangle / \langle V_x^B \rangle$ turns out to be a non-monotonic function of N_A/N_B , with a maximum at $N_A/N_B \approx 2$ (see Fig. 5).

V. CONCLUSIONS

We demonstrated that particles in a binary mixture can be effectively separated by using self-driven particles, or microswimmers, that move through the system. We analyzed the main features of the particle separation and explained mechanisms of different regimes including one with a velocity inversion. Our theoretical findings can be verified in experiments with microswimmers in colloidal binary mixtures. Indeed, the revealed regimes of particle flow separation are based on a rather general interplay between the interaction and the dynamical friction. In addition, in our model we used realistic experimental parameters. For example, our estimates for the “driving force” needed to observe the predicted behavior is on the order of (0.1-0.2)pN which agrees with the estimates for light-driven Janus particles in the experiments [40, 41]. Furthermore, the same experimental studies reported on: (i) the high control of the direction of motion of microswimmers (i.e., by employing various illumination patterns) and (ii) the tunability of the “driv-

ing force” of light-driven Janus particles (i.e., by tuning the intensity of the illumination). These two ingredients are of key importance for the possibility of experimental realization of the present theoretical findings. Moreover, the approach used in this work is also applicable to microrheology. The results of our study can be useful for mixture separation in biology and medicine.

VI. ACKNOWLEDGMENTS

This work was supported by the “Odysseus” Program of the Flemish Government and the Flemish Science Foundation (FWO-V1) (Belgium), by the National Natural Science Foundation of China (No. 11047111), the State Key Program of National Natural Science of China (No. 51135007), the Research Fund for the Doctoral Program of Higher Education of China (No. 20111415120002), and the Major State Basic Research Development Program of China (973) (No. 2009CB724201).

-
- [1] R. Haghgooie and P. S. Doyle, *Phys. Rev. E* **70**, 061408 (2004).
 - [2] A. Ricci, P. Nielaba, S. Sengupta, and K. Binder, *Phys. Rev. E* **74**, 010404(R) (2006).
 - [3] R. Haghgooie, C. Li, and P. S. Doyle, *Langmuir* **22**, 3601 (2006).
 - [4] T. R. Stratton, S. Novikov, R. Qato, S. Villarreal, B. Cui, S. A. Rice, and B. Lin, *Phys. Rev. E* **79**, 031406 (2009).
 - [5] R. Haghgooie and P. S. Doyle, *Phys. Rev. E* **72**, 011405 (2005).
 - [6] W. P. Ferreira, G. A. Farias and F. M. Peeters, *J. Phys.: Condens. Matter* **22**, 285103 (2010).
 - [7] Q.-H. Wei, C. Bechinger, and P. Leiderer, *Science* **287**, 625 (2000).
 - [8] C. Lutz, M. Kollmann, and C. Bechinger, *Phys. Rev. Lett.* **93**, 026001 (2004).
 - [9] A. Taloni and F. Marchesoni, *Phys. Rev. Lett.* **96**, 020601 (2006).
 - [10] K. Nelissen, V. R. Misko and F. M. Peeters, *EuroPhys. Lett.* **80**, 56004 (2007).
 - [11] G. Piacente and F. M. Peeters, *Phys. Rev. B* **72**, 205208 (2005).
 - [12] M. Köppl, P. Henseler, A. Erbe, P. Nielaba, and P. Leiderer, *Phys. Rev. Lett.* **97**, 208302 (2006).
 - [13] D. V. Tkachenko, V. R. Misko, and F. M. Peeters, *Phys. Rev. E* **80**, 051401 (2009).
 - [14] C. Reichhardt, C. Bairnsfather, and C. J. Olson Reichhardt, *Phys. Rev. E* **83**, 061404 (2011).
 - [15] C. Bairnsfather, C. J. Olson Reichhardt, and C. Reichhardt, *EuroPhys. Lett.* **94**, 18001 (2011).
 - [16] R. D. Astumian, *Phys. Rev. Lett.* **91**, 118102 (2003).
 - [17] R. Roth and D. Gillespie, *Phys. Rev. Lett.* **95**, 247801 (2005).
 - [18] J. Han and H. G. Craighead, *Science* **288**, 1026 (2000).
 - [19] P. S. Doyle, J. Bibette, A. Bancaud, and J.-L. Viovy, *Science* **295**, 2237 (2002).
 - [20] D. W. Trahan and P. S. Doyle, *Macromolecules* **44**, 383 (2011).
 - [21] Z. Siwy and A. Fuliński, *Phys. Rev. Lett.* **89**, 198103 (2002).
 - [22] Y. He, D. Gillespie, D. Boda, I. Vlassiuk, R. S. Eisenberg, and Z. S. Siwy, *J. Am. Chem. Soc.* **131**, 5194 (2009).
 - [23] A. Gopinathan and D. G. Grier, *Phys. Rev. Lett.* **92**, 130602 (2004).
 - [24] S. Savel’ev, A. L. Rakhmanov, and F. Nori, *Phys. Rev. B* **74**, 024404 (2006).
 - [25] S. Savel’ev and F. Nori, *Nat. Mater.* **1**, 179 (2002).
 - [26] S. Savel’ev, F. Marchesoni, and F. Nori, *Phys. Rev. Lett.* **91**, 010601 (2003).
 - [27] S. Savel’ev, F. Marchesoni, and F. Nori, *Phys. Rev. E* **70**, 061107 (2004).
 - [28] S. Savel’ev, F. Marchesoni, and F. Nori, *Phys. Rev. E* **71**, 011107 (2005).
 - [29] S. Savel’ev, F. Marchesoni, and F. Nori, *Phys. Rev. Lett.* **92**, 160602 (2004);
 - [30] W. Yang, K. Nelissen, M. Kong, Z. Zeng, and F. M. Peeters, *Phys. Rev. E* **79**, 041406 (2009).
 - [31] A. Engel, H. W. Müller, P. Reimann, and A. Jung, *Phys. Rev. Lett.* **91**, 060602 (2003).
 - [32] S. Savel’ev, V. R. Misko, F. Marchesoni and F. Nori, *Phys. Rev. B* **71**, 214303 (2005).
 - [33] D. Ertas, *Phys. Rev. Lett.* **80**, 1548 (1998).
 - [34] L. R. Huang, J. O. Tegenfeldt, J. J. Kraeft, J. C. Sturm, R. H. Austin, and E. C. Cox, *Nat. Biotechnol.* **20**, 1048 (2002).
 - [35] M. Berger, J. Castelino, R. Huang, M. Shah, and R. H. Austin, *Electrophoresis* **22**, 3883 (2001).
 - [36] A. Oudenaarden and S. G. Boxer, *Science* **285**, 1046 (1999).
 - [37] L. R. Huang, E. C. Cox, R. H. Austin, and J. C. Sturm, *Science* **304**, 987 (2004).

- [38] M. V. Gnann, I. Gazuz, A. M. Puertas, M. Fuchs, and Th. Voigtmann, *Soft Matter* **7**, 1980 (2011).
- [39] S. J. Ebbens and J. R. Howse, *Soft Matter* **6**, 726 (2010).
- [40] I. Buttinoni, G. Volpe, F. Kümmel, and C. Bechinger, Submitted to: *J. Phys.: Condens. Matter*; e-print arXiv:1110.2202v3 (2012).
- [41] G. Volpe, I. Buttinoni, D. Vogt, H.-J. Kümmerer, and C. Bechinger, *Soft Matter* **7**, 8810 (2011).
- [42] Q. Chen, J. K. Whitmer, S. Jiang, S. C. Bae, E. Luijten, and S. Granick, *Science* **331**, 199 (2011).
- [43] S. Berger, L. Ionov, A. Synytska, *Adv. Funct. Mater.* **21**, 2338 (2011).
- [44] A. Synytska, R. Khanum, L. Ionov, C. Cherif, and C. Bellmann, *ACS Appl. Mater. Interfaces* **3**, 1216 (2011).
- [45] T. R. Kline, W. F. Paxton, T. E. Mallouk, and A. Sen, *Angew. Chem. Int. Ed.* **44**, 744 (2005).
- [46] P. Tierno, R. Albalat, and F. Sagués, *Small* **6**, 1749 (2010).
- [47] K. Nelissen, B. Partoens, I. Schweigert and F. M. Peeters, *EuroPhys. Lett.* **74**, 1046 (2006).
- [48] U. M. Córdova-Figueroa and J. F. Brady, *Phys. Rev. Lett.* **100**, 158303 (2008).
- [49] U. M. Córdova-Figueroa and J. F. Brady, *Phys. Rev. Lett.* **103**, 079802 (2009).
- [50] M. B. Wan, C. J. Olson Reichhardt, Z. Nussinov, and C. Reichhardt, *Phys. Rev. Lett.* **101**, 018102 (2008).
- [51] B. ten Hagen, S. van Teeffelen, and H Löwen, *J. Phys.: Condens. Matter* **23**, 194119 (2011).
- [52] S. van Teeffelen and H Löwen, *Phys. Rev. E* **78**, 020101(R) (2008).
- [53] Taking into account rotational motion of a MS would lead to additional randomness (which is already present, due to the thermal stochastic term in Eq. (1)), in the trajectory of the MS. However, the preferable (average) direction of motion of the MS still can be controlled by employing illumination patterns.
- [54] V. R. Misko and F. M. Peeters, *Phys. Rev. B* **74**, 174507 (2006).
- [55] N. S. Lin, V. R. Misko, and F. M. Peeters, *Phys. Rev. Lett.* **102**, 197003 (2009).